

GNN-PMB: A Simple but Effective Online 3D Multi-Object Tracker without Bells and Whistles

Jianan Liu*, Liping Bai*, Yuxuan Xia, Tao Huang, *Senior Member, IEEE*,
Bing Zhu†, *Member, IEEE*

Abstract—Multi-object tracking (MOT) is among crucial applications in modern advanced driver assistance systems (ADAS) and autonomous driving (AD) systems. Most solutions to MOT are based on random vector Bayesian filters like global nearest neighbor (GNN) plus rule-based heuristical track maintenance. With the development of random finite set (RFS) theory, the RFS Bayesian filters have been applied in MOT tasks for ADAS and AD systems recently. However, their usefulness in the real traffic is open to doubt due to computational cost and implementation complexity. In this paper, it is revealed that GNN with rule-based heuristic track maintenance is insufficient for LiDAR-based MOT tasks in ADAS and AD systems. This judgement is illustrated by systematically comparing several different multi-point object filter-based tracking frameworks, including traditional random vector Bayesian filters with rule-based heuristical track maintenance and RFS Bayesian filters. Moreover, a simple and effective tracker, namely Poisson multi-Bernoulli filter using global nearest neighbor (GNN-PMB) tracker, is proposed for LiDAR-based MOT tasks. The proposed GNN-PMB tracker achieves competitive results in nuScenes test dataset, and shows superior tracking performance over other state-of-the-art LiDAR only trackers and LiDAR and camera fusion-based trackers.

Index Terms—Multi-Object Tracking, Random Vector-based Bayesian Filters, Random Finite Set based Bayesian Filters, GNN-PMB, LiDAR, Autonomous Driving

I. INTRODUCTION

MULTI-OBJECT tracking (MOT) is an integral and much-researched computational module for autonomous driving related applications [1]. According to the chronological process of detection and tracking, MOT can be categorized into track-before-detection [2], joint-detection-and-tracking [3], and track-by-detection. Track-by-detection is the process when outputs of an object detector across frames are connected by their corresponding track IDs, as shown by Fig. 1. The object detector provides the bounding box information. Then the multi-object tracker refines the information provided by the object detector, and assigns the appropriate ID to the bounding box. Depending on the sensor modalities employed, MOT can be further categorized as 2D MOT with camera [4][5], 3D MOT with LiDAR only [1][6][7][8], and 3D MOT with both camera and LiDAR

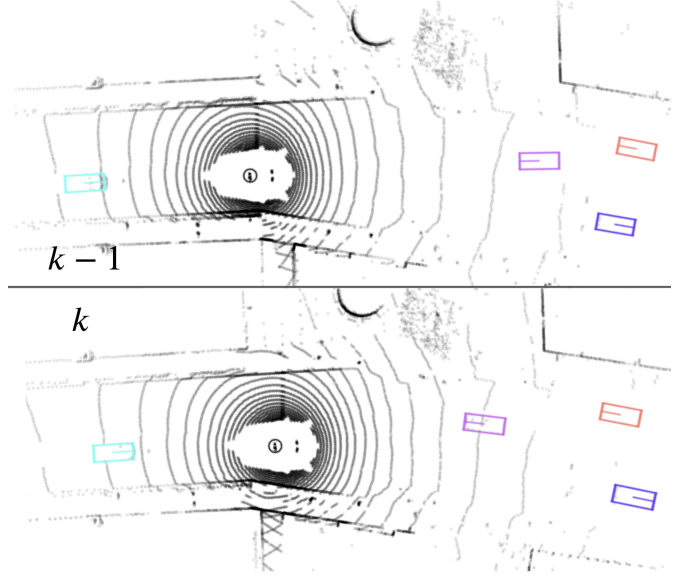


Fig. 1: Track-by-Detection 3D MOT using LiDAR: the outputs of the MOT filter over two consecutive frames (namely frame $k-1$ and frame k) are presented. The object surrounded by concentric circles is the ego vehicle. The grey dots are LiDAR point clouds presented in the bird-eye-view (BEV) frame. The coloured bounding boxes are the projection of 3D detected bounding boxes into the BEV frame. The orientation of a bounding box is indicated by the central line with half of the length. Bounding boxes with the same colour share the same track ID.

[9][10]. In this paper, track-by-detection 3D MOT with LiDAR is discussed.

Motivations of using multi-object tracker include: 1) the tracker assigns and maintains a unique track ID throughout the life cycle of a track; 2) the tracker rejects the false detection provided by the object detector; 3) the tracker sustains the track when the tracked object fails to be detected over consecutive frames; and 4) the tracker refines the information provided by the object detector. Essentially, a multi-object tracker is a state estimator, or equivalently, a filter. In this paper, the concepts "multi-object tracker", "tracker" and "filter" are equivalent.

Currently, researches in autonomous driving related MOT are conducted mainly in the computer vision community, where the proposed MOT strategies and algorithms are increasingly complicated. However, MOT is just one of the many computation modules in the autonomous driving pipeline, which consists of an object detection module, an MOT module, a trajectory prediction module, a motion planning module, and a control module. It is prohibitive for each module to be com-

*Both authors contribute equally to the work and are co-first authors.

†Corresponding author.

J. Liu is with Vitalent Consulting, Gothenburg, Sweden, and Silo AI, Stockholm, Sweden. Email: jianan.liu@vitalent.se, jianan.liu@silo.ai.

L. Bai and B. Zhu are with the School of Automation Science and Electrical Engineering, Beihang University, Beijing 100191, P.R. China. Email: bai_liping@buaa.edu.cn (L. Bai); zhubing@buaa.edu.cn (B. Zhu).

Y. Xia is with Department of Electrical Engineering, Chalmers University of Technology, Gothenburg 41296, Sweden. Email: yuxuan.xia@chalmers.se.

T. Huang is with College of Science and Engineering, James Cook University, Cairns, Australia. Email: tao.huang1@jcu.edu.au.

putationally demanding and time-consuming. Consequently, it is valuable to design a simple effective multi-objective tracker.

This paper proposes a simple and effective online 3D multi-object tracker based on random finite sets (RFSs) and the Poisson multi-Bernoulli filter using global nearest neighbor (GNN-PMB) tracker. This simple online tracker achieves state-of-the-art performance on the nuScenes 3D LiDAR-based MOT benchmark dataset. Main contributions of this paper are listed as follows:

- A systematic comparison in the nuScenes benchmark dataset among several commonly used Bayesian filters and the proposed GNN-PMB filter, is conducted for the first time according to the best of authors' knowledge. Such a systematic comparison of the real measured data provides a guideline for designing the tracking framework in practice.
- A simple and effective online LiDAR-based tracker, GNN-PMB, is proposed. It requires only the 2D coordinate information in the global frame as the input. The proposed tracker outperforms all the state-of-the-art trackers using LiDAR only, and the vast majority of state-of-the-art trackers use the fusion of LiDAR and camera in the nuScenes dataset for the 3D MOT task.
- The proposed GNN-PMB is designed in a unified and fairly simple framework. It does not require heuristic rules for track maintenance. It is simple to tune and more robust to detection deterioration than the GNN framework with lots of tricks and heuristics, which is widely employed by modern trackers in the practical ADAS and AD system.

The rest of the paper is arranged as follows. Section II discusses the related works of 3D LiDAR-based MOT in autonomous driving-related applications. In Section III, the important RFSs, the modelling assumptions, and the RFS Bayesian recursion are introduced. An overview and systematic study of typical Bayesian MOT filters are introduced in Section IV. The proposed GNN-PMB tracker is detailed in Section V. Some corresponding experimental results are presented and analysed in Section VI. Finally, the conclusion is drawn in Section VII.

II. RELATED WORKS

The advent of high-quality, publicly available LiDAR datasets prompted researches in LiDAR-based 3D MOT. The researches can be categorised into non-learning-based methods and learning-based methods.

A. 3D MOT with LiDAR Only

1) *LiDAR-based 3D MOT without Learning*: AB3DMOT [1] proposes a simple 3D Kalman filter for the LiDAR-based 3D MOT problem. The track-and-detection association is computed based on the 3D intersection over union (IoU) score [11], i.e., the track-and-detection association with the highest association score is regarded as the valid association scheme. This work establishes the baseline for the LiDAR-based 3D MOT problem by providing the code for new evaluation metrics. For example, its code is applied to evaluate the tracking challenge

on the nuScenes dataset. Probabilistic 3D MOT [6] applies Mahalanobis distance instead of 3D IoU as the score for track-and-detection association. It is the first time Mahalanobis distance was used in the 3D MOT problem, where better tracking results were achieved than those in AB3DMOT. SimpleTrack [7] uses 3D generalised intersection over union (GIoU) instead of 3D IoU as the track-and-detection score, and it applies a non-maximum suppression (NMS) preprocessing step to the detection information provided by the object detector. The combination of GIoU and NMS preprocessing improves the tracking result. ImmortalTracker [12] and PC3T [13] consider the similar idea, silently maintaining the tracks even when the tracks are no longer visible, and reducing the ID switches and fragmented tracks in tracking results. The aforementioned trackers terminate or initiate tracks based on hard-coded rules that might be too rigid for the MOT application. Score refinement is proposed in confidence-based 3D MOT [14] for track maintenance, where the tracker achieves a low ID switch score and track fragmentation score. RFS-M3 [15] firstly applies RFS-based methods, specifically PMBM filter, to the LiDAR 3D MOT problem. However, neither implementation details nor parameters are provided in [15]. Belief Propagation Tracker [8] poses the MOT problem in its factor graph representation, and uses sum-product message passing to compute the approximate marginal association probability iteratively. Although the Belief Propagation Tracker fails to achieve state-of-the-art performance, it is the first time that this method has been applied to the 3D LiDAR MOT problem.

2) *LiDAR-based 3D MOT with Learning*: There are two ways to incorporate learning into the MOT problem. The first way is integrating detection into the process. For instance, SimTrack [16] proposed an end-to-end trainable model for joint detection and tracking from raw point clouds. The second way is the feature-based track-and-detection association. A graph structure is designed in OGR3MOT [17] to jointly process detection and tracking in an online manner. The graph structure is a Neural Message Passing network for fully trainable data association. Neural enhanced belief propagation (NEBP) tracker [18] is an update to the Belief Propagation Tracker [8], proposing a belief propagation scheme complemented by a learned neural network. The NEBP tracker achieves superior tracking performance over its non-learning-based counterpart, namely the Belief Propagation tracker.

B. 3D MOT with LiDAR and Camera Fusion

Besides LiDAR only approaches for 3D MOT, fusion of LiDAR and camera is another strategy which is commonly used for 3D MOT. In Probabilistic 3D Multi-Modal MOT [9], the system fuses features from 2D images and 3D LiDAR point clouds to capture an object's appearance and geometric information. Then the system uses a metric that combines the Mahalanobis and feature distances for the track-and-detection association. By incorporating the camera information, the Probabilistic 3D Multi-Modal MOT tracker achieves better tracking results than the Probabilistic 3D multi-object tracker which only uses 3D LiDAR detection as input. EagerMOT [10] further improves the tracking performance by utilising

the detection distance between the camera-based and the LiDAR-based detection. AlphaTrack [19] improves the tracking performance by adding a feature extractor along with the side of the object detector. The feature extractor takes image information and the LiDAR point cloud information as inputs, and provides information for a more accurate track-and-detection association.

III. BACKGROUND

In RFS-based methods, object states and measurements are represented in the form of finite sets. The multi-object state at time step k is denoted as $X_k = \{x_k^1, \dots, x_k^{n_k}\}$ where $x_k^i \in \mathbb{R}^{n_x}$ is the i -th single-object state and the set cardinality is $|X_k| = n_k$. The set of measurements at time step k is denoted as Z_k , and the sequence of all the measurement sets received so far up to and including time step k is Z^k .

A. Important Random Finite Sets

The two families of RFSs that have prominent roles in the RFSs-based methods are the Poisson point process (PPP) and the Bernoulli process. A PPP with intensity function $\lambda(\cdot)$ has RFS density

$$f^{ppp}(X) = e^{-\int \lambda(x) dx} \prod_{x \in X} \lambda(x) \quad (1)$$

where $|X|$ is Poisson distributed with mean $\bar{\lambda} = \int \lambda(x) dx$. A Bernoulli process with existence probability r and existence-conditioned probability density function (PDF) $f(\cdot)$ has RFS density

$$f^{ber}(X) = \begin{cases} 1 - r & X = \emptyset \\ r f(x) & X = \{x\} \\ 0 & \text{otherwise} \end{cases} \quad (2)$$

where $|X|$ is Bernoulli distributed with parameter r . A multi-Bernoulli (MB) RFS X is the union of a finite number of independent Bernoulli processes X_1, \dots, X_n , and its density is

$$f^{mb}(X) = \sum_{\uplus_i^n X_i = X} f_i^{ber}(X_i) \quad (3)$$

where \uplus denotes the disjoint union and $f_i^{ber}(\cdot)$ is the density of the i -th Bernoulli component.

B. Bayesian Filtering Recursion

In Bayesian MOT filtering, we are interested in computing multi-object posterior $f_{k|k}(X_k|Z^k)$, which captures all the information of the set X_k of objects at time step k conditioned on all the measurements received so far. In particular, this is done by recursively applying the Chapman-Kolmogorov prediction

$$\begin{aligned} & f_{k|k-1}(X_k|Z^{k-1}) \\ &= \int \Phi_{k|k-1}(X_k|X_{k-1}) f_{k-1|k-1}(X_{k-1}|Z^{k-1}) \delta X_{k-1} \end{aligned} \quad (4)$$

and the Bayes update

$$f_{k|k}(X_k|Z^k) \propto G(Z_k|X_k) f_{k|k-1}(X_k|Z^{k-1}), \quad (5)$$

where $\int f(X) \delta X$ is the set integral [20], $\Phi_{k|k-1}(X_k|X_{k-1})$ is the multi-object transition density, and $G(Z_k|X_k)$ is the multi-object measurement likelihood.

C. Standard Multi-object Models

In this paper, we use the standard multi-object dynamic model $\Phi_{k|k-1}(X_k|X_{k-1})$ [20], which is based on the following assumptions:

- Single object with state x_{k-1} at time step $k-1$ moves to a new state x_k with a Markov transition density $\phi(x_k|x_{k-1})$.
- Single object with state x_k at time step k has a probability $P^S(x_k)$ of leaving the sensor's field-of-view.
- New objects X_k^b at time step k appear in the sensor's field-of-view according to a PPP with intensity $\lambda_k^b(\cdot)$.
- The appearing/disappearing of newborn/existing objects, and the object motions are conditionally independent of the previous multi-object state X_{k-1} .
- The set X_k of objects at time step k is the union of the set X_k^e of existing objects at time step k and the set X_k^b of newborn objects, i.e., $X_k = X_k^e \cup X_k^b$.

The multi-object transition density $\Phi_{k|k-1}(X_k|X_{k-1})$ can be written as a convolution of a PPP density for newborn objects X_k^b and a multi-Bernoulli density for existing objects X_k^e

$$\begin{aligned} & \Phi_{k|k-1}(X_k|X_{k-1}) \\ &= \sum_{X_k^b \uplus X_k^e = X_k} f_k^{ppp}(X_k^b) f_{k|k-1}^{mb}(X_k^e|X_{k-1}). \end{aligned} \quad (6)$$

In addition, we use the standard multi-object measurement model $G(Z_k|X_k)$ for point objects [20], which is based on the following assumptions:

- The set Z_k of measurements at time step k consists of measurements Z_k^o generated by the set X_k of objects and clutter measurements Z_k^c , i.e., $Z_k = Z_k^o \cup Z_k^c$.
- The two sets of measurements Z_k^o and Z_k^c are statistically independent.
- No measurement is generated by more than one object.
- Given a set X_k of objects, each object $x_k \in X_k$ is either detected with probability $P^D(x_k)$ and generates a single measurement z_k with measurement likelihood $g(z_k|x_k)$, or misdetected with probability $1 - P^D(x_k)$.
- The set Z_k^c of measurements is a PPP with intensity $\lambda_k^c(\cdot)$.

The multi-object measurement likelihood $G(Z_k|X_k)$ can be written as a convolution of a PPP density for clutter measurements Z_k^c and a multi-Bernoulli density for object-oriented measurements Z_k^o

$$G(Z_k|X_k) = \sum_{Z_k^c \uplus Z_k^o = Z_k} f_k^{ppp}(Z_k^c) f_k^{mb}(Z_k^o|X_k). \quad (7)$$

IV. A SYSTEMATIC STUDY OF BAYESIAN MOT METHODS

In this section, we present a systematic study of common Bayesian MOT methods available in the literature from two aspects: 1) track maintenance, and 2) approximation methods for computationally tractability.

A. Global and Local Hypotheses

The main challenge of MOT is the data association problem, which is due to the unknown correspondence between objects and measurements, and therefore we begin by giving a unified terminology of data association hypotheses.

Suppose we consider the data associations at time step k . A local hypothesis is defined as a pair of object-to-measurement association at time step k , and a global hypothesis is a valid collection of local hypotheses, explaining the association of every object and measurement at time step k .

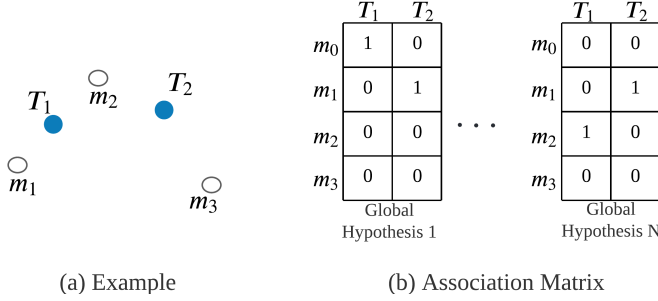


Fig. 2: An example illustrating the local and global hypotheses. Given the objects and measurements in (a), examples of global hypotheses, represented using association matrices are shown in (b).

To further explain the details of local and global hypothesis, let us consider the example illustrated in Fig. 2 where there are two objects T_1, T_2 , and three measurements m_1, m_2, m_3 . The global hypotheses describing their associations are represented using binary association matrices where each entry represents a possible local hypothesis and we use dummy notation m_0 for misdetections. For every association matrix, it satisfies that 1) each column must sum to one, and 2) each row must sum to one or zero. An all-zero row (except for m_0) means that the corresponding measurement belongs to the clutter. For the two global hypotheses shown in Fig. 2 (b), Global hypothesis 1 represents that object T_1 is misdetected and object T_2 is associated with measurement m_1 , whereas Global hypothesis N represents that object T_1 is associated to measurement m_2 and object T_2 is associated to measurement m_1 .

B. Different MOT Methods

Bayesian MOT methods in the literature can be generally categorised into 1) MOT methods based on RFSs and 2) MOT methods based on random vectors.

1) *Vector-based MOT Methods*: Vector-based MOT methods describe the multi-object states and measurements by random vectors, and the most representative methods are the global nearest neighbor (GNN) filter [21], the joint probabilistic data association (JPDA) filter [22][23], and the multiple hypothesis tracking (MHT) filter [24]. Due to the unknown data associations, the number of global hypotheses increases hyper-exponentially over time. The GNN filter only keeps the most likely global hypothesis at each time step. The JPDA filter first computes the (approximate) marginal object-to-measurement association probabilities and then it merges local hypotheses corresponding to the same object. MHT seeks to find the most likely global hypothesis over a sliding window

of consecutive time steps, which involves the propagation of multiple global hypotheses over time.

2) *Set-based MOT Methods*: Set-based MOT methods describe the multi-object states and measurements by RFSs. There are a variety of RFSs-based MOT methods in the literature. Early developments include methods that avoid explicitly handling the data association uncertainty, such as the probability hypothesis density (PHD) filter [25] and the cardinalized PHD (CPHD) filter [26] using moment approximations. The PHD and CPHD filters approximate the multi-object posterior by a PPP and an i.i.d. cluster process, respectively, both in the sense of minimising the Kullback-Leibler divergence. The CPHD filter is computationally heavier than the PHD filter, but it yields better performance when the signal-to-noise ratio is low.

A significant trend in RFSs-based MOT is the development of filters based on multi-object conjugate priors, which means that the multi-object posterior has the same functional form as the predicted distribution (and the prior). A typical example is the Poisson multi-Bernoulli mixture (PMBM) filter [27], which gives the closed-form solution for the standard multi-object models introduced in Section III-C. In the PMBM filter, both the prediction and the update preserve the PMBM form of the density without approximation:

$$f_{k|k'}^{pmbm}(X_k|Z^{k'}) = \sum_{X_{k'}^u \cup X_{k'}^d = X_{k'}} f_{k|k'}^{ppp}(X_{k'}^u) f_{k|k'}^{mbm}(X_{k'}^d), \quad (8)$$

$$f_{k|k'}^{mbm}(X_{k'}^d) = \sum_{h=1}^{H_{k'}} w_{k'}^h f_{k|k'}^h(X_{k'}^d) \quad (9)$$

where $k' \in \{k-1, k\}$. In (8), the set $X_{k'}^u$ of undetected objects that have not yet been detected is described by a PPP, whereas the set $X_{k'}^d$ of detected objects that have been detected at least once is described by a multi-Bernoulli mixture (MBM). In the MBM (9), each multi-Bernoulli component corresponds to a unique global hypothesis for the detected objects. The h -th multi-Bernoulli component has density $f_{k|k'}^h(\cdot)$ and weight w^h , which satisfies that $\sum_{h=1}^{H_{k'}} w_{k'}^h = 1$. If there is only a single multi-Bernoulli component in (9), i.e., when $H_{k'} = 1$, then the PMBM filter reduces to a PMB filter [28].

C. Track Maintenance

For practical implementations of Bayesian MOT methods, we need efficient track maintenance scheme for tracking a time-varying number of objects. In this paper, a track is defined as a sequence of local hypothesis densities at consecutive time steps that correspond to the same object. Track maintenance refers to the process where a track is initiated, sustained, and terminated. In what follows, we discuss the track maintenance scheme for vector-based and set-based MOT methods separately.

1) *Vector-based MOT Methods*: Vector-based MOT methods can explicitly maintain track continuity by associating an object state estimate with a previous state estimate; however, they mainly rely on heuristic methods to take into account the appearance/disappearance of new/existing objects. A commonly used rule for track maintenance is called M/N logic.

Specifically, a tentative track is initiated when a measurement is not associated with any existing tracks, and this tentative track is terminated confirmed if there are M measurement associations out of N consecutive time steps. The termination of tracks follows a similar procedure. Alternatively, one can use track-score-based logic for track maintenance by performing hypothesis test.

2) *Set-based MOT Methods*: The RFS formalism facilitates the modelling of the appearance/disappearance of new/existing objects in a Bayesian setting. For example, in the PMBM and PMB filters, we only extract object state estimates from Bernoulli components with existence probability above a certain threshold. However, in RFS-based MOT methods, time sequences of tracks cannot be constructed easily as the multi-object states are order independent. One approach to maintain track continuity is to add unique labels to the object states and form tracks by linking object state estimates with the same label [29]. A more appealing approach to solve the track building problem is by computing multi-object densities on sets of trajectories [30], and a typical example is the trajectory PMBM filter [31]. We note that the prediction and update in the PMBM filter can be viewed as an efficient method for calculating the time marginals of the RFS of trajectories [31]. Therefore, track continuity in the PMBM and PMB filters can be established using metadata; the detailed procedure will be described in Section V-B2.

D. Approximations for Computational Tractability

Practical MOT implementations need efficient approximations to keep the computational complexity at a tractable level. The approximations methods can be categorised into local and global hypothesis reductions.

1) *Local Hypothesis Reduction*: To limit the number of local hypotheses, the most commonly used strategy is gating. Specifically, for a predicted local hypothesis density we only consider the associations of measurements that are inside its gated region, so that the number of updated local hypotheses can be reduced.

Different MOT methods use different techniques for further reducing the number of local hypotheses after the update. In MHT, the number of local hypotheses is limited by implementing N -scan pruning [32] or by pruning local hypotheses with low scores. In Gaussian implementations of PHD and CPHD filters, Gaussian mixture reduction is performed for the PPP intensity by pruning components with small weights and merging similar components. In PMBM and PMB filters, we need to prune Gaussian components in the PPP intensity with small weights and Bernoulli components with small existence probabilities.

2) *Global Hypothesis Reduction*: The key to global hypothesis reduction relies on how to efficiently solve the data association problem. For solving the multi-scan data association problem, typical solutions include Lagrangian relaxation [32] and Markov chain Monte Carlo sampling [33]. For MOT methods considering the single-scan data association problem, the most likely global hypothesis can be obtained by solving a 2D assignment problem using, e.g., the Hungarian algorithm

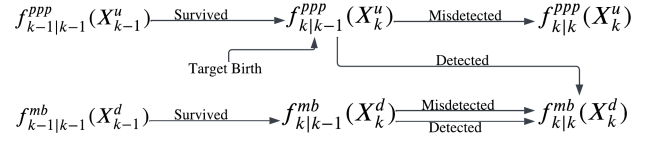


Fig. 3: PMB Bayesian recursion consists of the recursion of PPP and the recursion of MB.

[34]; and the K best global hypotheses can be obtained using Murty's algorithm [34]. The merging step in the JPDA filter and the track oriented PMB (TO-PMB) filter makes use of the (approximate) marginal association probabilities; they can be either computed using the K best global hypotheses obtained from Murty's algorithm or directly obtained using loopy belief propagation (LBP) [35] without explicit enumeration of global hypotheses.

V. METHOD

According to the analysis presented by [36][37], the PMBM filter results in the best performance under simulation circumstances. However, because the number of objects in a real-world scenario can be large and the number of corresponding measurements per frame can be even greater, the hypothesis management which propagates K best global hypotheses used by the PMBM filter could be computationally intensive, especially for frames with the greatest number of measurements. To overcome the computational burden introduced in the hypothesis management part of PMBM filter, one way is to employ TO-PMB filter [28] which propagates only the approximated global hypothesis by using messaging passing, yet the messaging passing step is still computationally demanding. In this paper, we choose another way which only propagates the most likely global hypothesis for our proposed tracker, in which the PMBM recursion is also reduced as PMB recursion as illustrated in Fig. 3 but would require much lower computations. Since such hypothesis management step is similar to the GNN filter, our proposed tracker is named as GNN-PMB. We will explain the implementation details of the proposed GNN-PMB tracker for LiDAR-based 3D MOT as the follows.

A. Basic Parameters for the GNN-PMB Tracker

There are several parameters which serve as the basic components of proposed GNN-PMB, we will discuss each of them in this subsection.

1) *Project a 3D Bounding Box to a Point in BEV*: The detected 3D bounding boxes, as the measurements of possible objects, would be utilized as input to the tracker. Although the available information of the 3D bounding boxes provided by the LiDAR object detector includes the following: x , y , and z coordinate in the global frame, bounding box size, orientation, velocity, detection score, and classification, the proposed tracker only requires the x and y coordinate in the global frame as input to keep the tracker as simple as possible. Other information provided by the 3D LiDAR object detector is propagated without filtering.

2) *Gating Distance*: Gating, which prunes away all the detected bounding boxes with a distance to the center point of predicted tracks smaller than a threshold, before organizing the possible local hypotheses for each track. The distance for gating can be defined by using different metrics, e.g., Euclidean distance, the 2D IoU, the 2D GIoU, or the 2D Mahalanobis distance, etc. The 2D Mahalanobis distance which incorporates the uncertainty information, while easier to compute than the 2D IoU and the 2D GIoU, is chosen as the distance for gating. It is defined by

$$d = \sqrt{(z_1 - z_2)^T \mathbf{P}^{-1} (z_1 - z_2)}, \quad (10)$$

where z_1 and z_2 are two points from the same distribution with covariance matrix \mathbf{P} . And the gating threshold for the proposed GNN-PMB filter is set to be $\sqrt{50}$ in 2D Mahalanobis distance.

3) *Association Likelihood Score*: The association likelihood score which denotes the how likely a possible local hypothesis between a detection and an object can occur, is applied to organize the cost matrix for hypothesis management which will be explained in **V-B1**. In the proposed GNN-PMB filter, the association likelihood score for a certain local hypothesis is defined as its multivariate Gaussian distribution, given by

$$\text{MVG}(z, m, \mathbf{P}) = \frac{1}{2\pi} |\mathbf{P}|^{-\frac{1}{2}} \exp^{-\frac{1}{2}(z-T)^T \mathbf{P}^{-1} (z-T)}, \quad (11)$$

where z is the 2D position of detection, and T is the 2D position of a track. \mathbf{P} is the covariance matrix of the distribution of T .

4) *Probability of Detection*: Section As specified in **III-C**, the probability of detection of a given object x is denoted by $P^D(x_k)$, and the probability of misdetection of a given object x is denoted by $1 - P^D(x_k)$. To better capture the likelihood of every detected bounding box in the dynamic environment, $P^D(x_k)$ is specifically chosen as detection score of each detected bounding box provided by object detector, rather than being set as a constant value.

5) *Clutter Rate*: The clutter generation process is a PPP with intensity $\lambda_k^c(\cdot)$, as shown in section **III-C**. To keep the computation as simple as possible, it is assumed that a constant expected number of clutter would be generated uniformly across the FoV. Therefore, the clutter intensity is defined as the expected number of clutters over the area of FoV. For the proposed GNN-PMB tracker, the clutter rate is set to be 0.001 over the area of FoV.

6) *Survival Probability*: The survival probability of an object, $P^S(x_k)$, conducts how likely an object will remain for the next frame. Correspondingly, disappearance of an object can be expressed as an i.i.d Markov processes with probability $1 - P^S(x_k)$. Theoretically, the $P^S(x_k)$ should be defined in terms of the position of object x_k . For instance, the disappearance of an object is most likely to occur around the peripheries of the FoV. However, $P^S(x_k)$ is set to be a uniform P_s in order to keep the computation as simple as possible. In this paper, the P_s of the proposed GNN-PMB tracker is set to be 0.7.

7) *Pruning Threshold of Existence Probability*: To lower the computational demand, all the Bernoulli components with an existence probability lower than the pruning threshold need to be eliminated. The pruning threshold of existence probability is set to be $1e-5$ for proposed GNN-PMB tracker, since the threshold should be small enough to retain the Bernoulli components for multiple frames before it is discarded.

B. Hypothesis Management and Track Maintenance for GNN-PMB Tracker

1) *Hypothesis Management*: Hypothesis management procedure, which is illustrated in Fig. 4, is one of the core modules for the proposed GNN-PMB tracker. A cost matrix is formed with the most likely global hypothesis at time $k - 1$, with each element representing the cost of every local hypothesis, denoted by the negative logarithm of the association probability score. The cost matrix is then subjected to the Hungarian algorithm, which selects the most likely global hypothesis at time k .

2) *Track Maintenance*: As another critical part of the proposed GNN-PMB tracker, track maintenance is implemented using meta-data maintained by every Bernoulli component. Suppose a measurement is assigned to its corresponding new Bernoulli component instead of an existing one. In that case, the new Bernoulli component would be output as a valid object, and the object ID is calculated by adding one to the current maximum ID. The new ID is stored as metadata to the new Bernoulli component. For the situation that measurement is associated with an existing Bernoulli component in the most likely global hypothesis, the Bernoulli component would be output as an existing object, and the ID of the object remains the same as the one for the existing Bernoulli component.

C. Other Tunable Parameters for the GNN-PMB Tracker

Other than the basic parameters, there is also the other set of key parameters which highly influence the performance of the proposed GNN-PMB tracker. In this section, the definition for each of these parameters would be introduced, and the detailed ablation studies for each of them would be detailed in Section **VI-D**.

1) *Detection Score Threshold*: Detection score threshold is a predetermined threshold to prune the input of tracker. For instance, a detection score threshold of 0.5 means that only detected bounding boxes with a detection score higher than 0.5 would be used as input to the MOT tracker.

2) *Non-maximum Suppression (NMS) Threshold*: The object detector often creates multiple bounding boxes around the same object. However, only one detection is required for each object. Non-max suppression is used to suppress the less likely bounding boxes. The NMS score is implemented as the 3D-IoU [11] score in this paper. If there are multiple bounding boxes whose 3D-IoU exceeds the specified NMS threshold, only the bounding boxes with the highest detection score would be kept as the input to tracker.

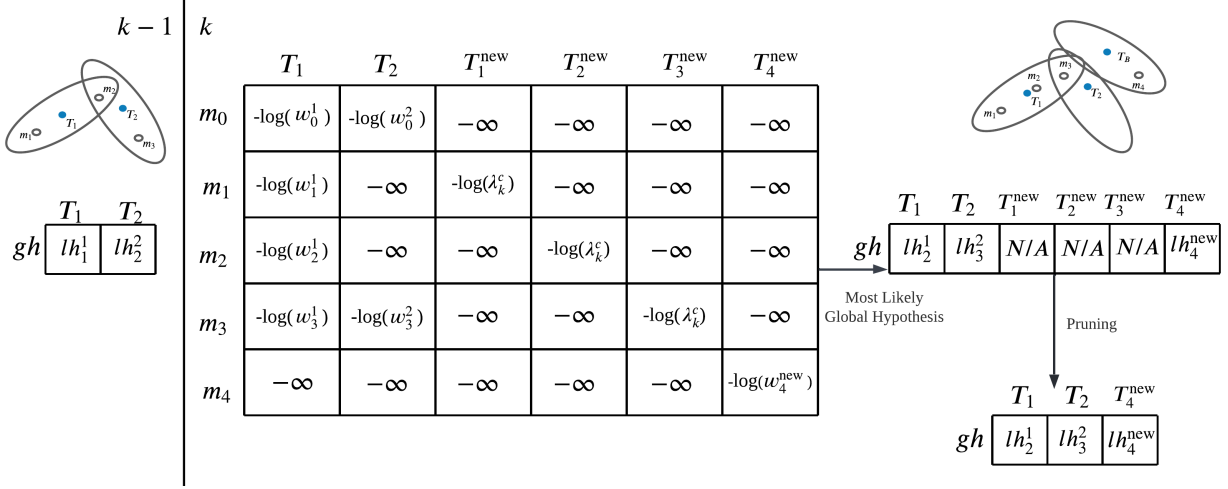


Fig. 4: The Hypothesis Management Procedure of GNN-PMB Tracker. A cost matrix is generated based on the most likely global hypothesis at time $k - 1$, and then propagated to current frame k . At frame k , the cost matrix is organized, by setting every cost element for local hypotheses within the gated area as negative logarithm of the association likelihood score of that local hypothesis, and cost element for local hypotheses outside the gated area as infinity. Then the most likely global hypothesis at frame k is selected based on this cost matrix. The example in the figure is the same as the one presented in earlier section, where lh_m^t indicates the local hypothesis with measurement m and object t , gh stands for global hypothesis, $\lambda_k^c(\cdot)$ is the clutter intensity and w is the likelihood score of the local hypothesis.

3) *Poisson Birth Density*: As introduced in Section III-C, the object birth process is modelled by PPP. The cardinality is distributed according to a Poisson distribution with intensity $\lambda_k^b(\cdot)$. In this paper, $\lambda_k^b(\cdot)$ is implemented as an unnormalised Gaussian mixture with identical weight, and the initial covariance matrix P_0 is identical for all the Gaussian components. Therefore, the weight of the Gaussian distribution and the initial covariance matrix P_0 need to be tuned in order to specify the Poisson birth density.

4) *Extraction Threshold*: For the GNN-PMB tracker, the detected multi-object state is modelled by MB RFS density. Each Bernoulli RFS density has its corresponding existence probability. Only the Bernoulli components with an existence probability higher than the specified extraction threshold are considered valid objects for a given frame. Bernoulli RFS density with an existence probability lower than the specified extraction threshold would be silently maintained until the existence probability falls below the pruning threshold.

VI. EXPERIMENTS AND ANALYSIS

A. Dataset

There are four major LiDAR-based 3D detection and tracking benchmark datasets, namely KITTI [38], Waymo [39], nuScenes [40], and Argoverse [41]. The experiments are conducted with the nuScenes benchmark dataset. The nuScenes dataset is chosen due to that: the annotation of nuScenes is manually validated; the nuScenes tracking challenge has the more 3D LiDAR-based MOT submissions than does the Waymo 3D tracking challenge; and The nuScenes tracking challenge evaluation process defines distance as the Euclidean distance, as opposed to the 3D-IoU used by the Waymo challenge. Euclidean distance would provide a fairer tracking evaluation for the proposed GNN-PMB tracker because only the x and y coordinate in the global frame is used as the input to the tracker.

B. Evaluation Metrics

Multi-object tracking accuracy(MOTA) and multi-object tracking precision(MOTP) are the most widely used metrics for MOT evaluation [42]. To define MOTA and MOTP, some key secondary metrics are introduced in Fig. 5. Mostly tracked (MT) Tracks are tracks with more than 80% TP detection. Mostly lost (ML) Tracks are tracks with less than 20% TP detection. The detailed definitions of secondary metrics can be found on the organiser's website ¹.

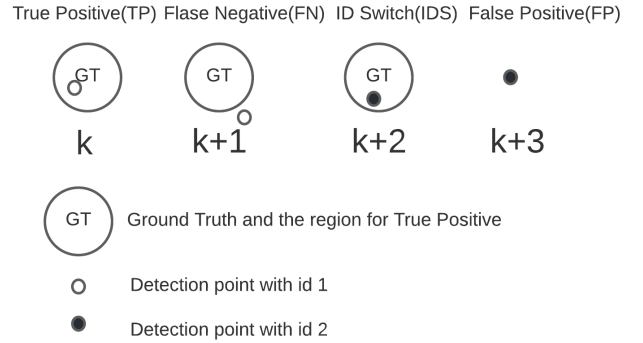


Fig. 5: Tracking evaluation metrics. This figure explains the definition of TP, FN, IDS and FP. True positive (TP) is the number of detection that fall within the valid region of its corresponding ground truth. False negative (FN) is the number of detection that fall outside the valid region of its corresponding ground truth. ID switch (IDS) is the number of detection that fall within the valid region of its corresponding ground truth, but the IDs assigned to the detection differ from that of the previous frame. False positive (FP) is the number of detection not associated with any ground truth. For the nuScenes dataset, the valid region is defined as a region around the ground truth position with a maximum Euclidean distance of 3.

¹<https://www.nuscenes.org/tracking>

MOTA of a given frame is defined by equation

$$\text{MOTA} = 1 - \frac{\sum \text{FN} + \text{FP} + \text{IDS}}{\text{GT}}, \quad (12)$$

where GT denotes the number of ground truth.

MOTP of a given frame is defined by

$$\text{MOTP} = \frac{\sum_i d_i}{\text{TP}}, \quad (13)$$

where d_i is the 3D Euclidean distance between the i^{th} TP detection position and its corresponding ground truth position.

However, the nuScenes tracking challenge does not use MOTA and MOTP as the primary evaluation metrics for the tracking performance. The challenge differentiates tracking results based on the average multi-object tracking accuracy (AMOTA).

To define AMOTA, the tracking score and the recall must be defined first. The object detector assigns a detection score between 0 and 1 to each bounding box. The score indicates the likelihood of the identified classification. For instance, a 3D bounding box might be assigned a detection score of 0.3 for it to be a bounding box for a car, and a score of 0.1 for it to be a bounding box for a truck. A tracking score is an object prediction score between 0 and 1 for the class identified. For the trackers evaluated in this paper, the tracking score is the same as the detection score.

The tracking score threshold for the AMOTA calculation is dynamically computed for each tracking result. For instance, for a given tracking result, the first recall greater than 0.1 is 0.104. It appears when the tracking score threshold is set to be 0.75. The highest recall is 0.85. It appears when the tracking score threshold is set to be 0.11. The n evaluated recalls are evenly spaced between 0.104 and 0.85, and the corresponding tracking score threshold would be used to evaluate secondary metrics under that recall. Of the evenly spaced recalls between 0.104 and 0.85, the recall with the highest corresponding MOTA would be used to generate all the secondary metrics of this tracking result.

Recall of a given tracking score threshold is defined by

$$r(ts) = \frac{\text{TP}_{ts}}{\text{GT}}, \quad (14)$$

where ts is the tracking score threshold. TP_{ts} is the number of True Positives when only detection with a tracking score higher than a specified tracking score threshold is considered valid.

The objective of AMOTA is to evaluate the tracking performances under different recalls. For a given frame, AMOTA is defined by

$$\text{AMOTA} = \frac{1}{n-1} \sum_{r \in \{\frac{1}{n-1}, \frac{2}{n-1}, \dots, 1\}} \text{MOTAR} \quad (15)$$

where n is the number of evaluated recalls, and r is the recall. For the nuScenes dataset, n is specified to be 40.

The MOTAR is the MOTA under a given recall. It is defined by

$$\text{MOTAR} = \max(0, 1 - \frac{\text{IDS}_r + \text{FP}_r + \text{FN}_r - (1-r) \times \text{GT}}{r \times \text{GT}}) \quad (16)$$

where IDS_r is the number of identity switches under that recall, FP_r is the number of false positives under that recall, and FN_r is the number of false negatives under that recall.

Another key metric used by nuScenes is AMOTP. For a given frame, AMOTP is defined by

$$\text{AMOTP} = \frac{1}{n-1} \sum_{r \in \{\frac{1}{n-1}, \frac{2}{n-1}, \dots, 1\}} \frac{\sum_i d_i}{\text{TP}}, \quad (17)$$

where d_i is the Eclidean distance between the i^{th} TP detection position and its corresponding ground truth position.

C. Comparisons among Different Bayesian Filters

As explained in section IV, a systematical study of different Bayesian filters has been investigated. Accordingly, the performance of all the evaluated Bayesian filters which are presented in TABLE I, will be discussed in this section. All the secondary metrics, i.e., MT, ML, TP, FP, FN, IDS, FRAG, are evaluated under the recall with the highest MOTA score.

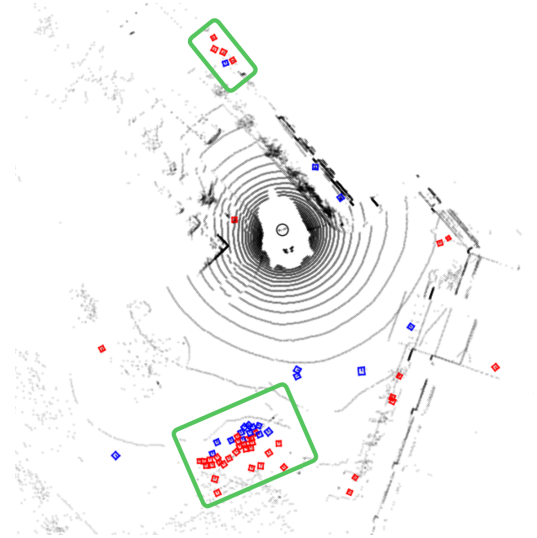


Fig. 6: Erroneous Measurement Model Assumption. The measurement model assumes that the clutter generation process is independent of the generation process of the valid detection. This figure demonstrates a case that this modelling assumption is violated. In this figure, the bounding boxes are taken directly from the object detector to show the clutter distribution. The grey dots are the LiDAR point clouds. The blue bounding boxes are the valid detection, and the red bounding boxes are the clutter. The detected object classification is pedestrian. The clutter generation process is coupled with the generation process of the valid detection in this frame. This observation is particularly true in the region enclosed by a green rectangle. The two regions contain valid detection, and the clutter are distributed around the valid detection.

1) *Quality of Detection Input*: Understanding how the tracking performance would change with detector input of varying qualities is important. To this end, the detection files provided by three different object detectors are used in our experiment. According to the nuScenes LiDAR-based detection challenge leaderboard, the rankings for the CenterPoint detector, the Megvii detector, and the PointPillars detector are 2, 36, and 59, respectively. The CenterPoint detection result

TABLE I: Tracking Results of Different LiDAR based Object Detectors and Bayesian Tracker Frameworks on nuScenes Validation Set.

Tracker	Detector	AMOTA \uparrow	AMOTP \downarrow	MT \uparrow	ML \downarrow	TP \uparrow	FP \downarrow	FN \downarrow	IDS \downarrow	FRAG \downarrow
GNN	PointPillars	0.251	1.403	1924	2158	50631	11776	45334	5932	2579
GNN	Megvii	0.509	0.881	3323	1722	67774	10759	29703	4420	1209
GNN	CenterPoint	0.603	0.735	3725	1447	72192	11767	25076	4629	1236
JPDA	Any	N/A	N/A	N/A	N/A	N/A	N/A	N/A	N/A	N/A
PHD	PointPillars	0.17	1.472	1443	2581	35583	42811	52241	14073	4728
PHD	Megvii	0.268	1.201	478	4670	17298	6501	79652	4947	3365
PHD	CenterPoint	0.313	1.114	835	3403	18856	39724	67996	15045	6071
CPHD	Any	N/A	N/A	N/A	N/A	N/A	N/A	N/A	N/A	N/A
TO-PMB	PointPillars	0.185	1.380	2474	2232	56685	19096	44444	768	857
TO-PMB	Megvii	0.294	0.926	2429	3162	49827	18613	51722	348	403
TO-PMB	CenterPoint	0.324	0.812	2737	2955	53982	15382	47433	482	449
PMBM	PointPillars	0.269	1.260	2709	2311	59250	12060	40800	1847	843
PMBM	Megvii	0.577	0.739	4314	1528	79094	13536	21829	974	406
PMBM	CenterPoint	0.645	0.600	4591	1349	82480	14608	18234	1183	403
GNN-PMB	PointPillars	0.311	1.231	2754	2236	60929	9993	39945	1023	769
GNN-PMB	Megvii	0.619	0.716	4314	1552	79434	11710	21955	508	372
GNN-PMB	CenterPoint	0.707	0.560	4608	1347	83134	12362	18113	650	345

\uparrow The upper arrow indicates that better performance is registered with higher score, same for the following tables.

\downarrow The lower arrow indicates that better performance is registered with lower score, same for the following tables.

TABLE II: Ablation Study of Filter Parameters. This table indicate how the tracking result changes with different parameters.

Parameters		Value	AMOTA \uparrow	AMOTP \downarrow	RECALL \uparrow	MT \uparrow	ML \downarrow	TP \uparrow	FP \downarrow	FN \downarrow	IDS \downarrow	FRAG \downarrow
Detection		0.1	0.707	0.559	0.738	4606	1353	83088	12300	18167	642	341
Score		0.2	0.672	0.705	0.693	4391	1414	80971	9198	20318	608	328
Threshold		0.3	0.625	0.834	0.659	4266	1199	80601	9965	20564	732	500
NMS		0.1	0.707	0.560	0.730	4611	1329	83057	12491	18082	758	333
Threshold		0.98	0.680	0.572	0.715	4513	1424	81830	13240	19267	800	333
Poisson	Weight of	0.0001	0.626	0.764	0.653	4415	1588	81039	14055	20254	604	429
		0.001	0.702	0.555	0.729	4510	1533	82235	14171	19101	561	351
Birth	Gaussian Components	0.01	0.703	0.559	0.729	4618	1383	83128	13714	18202	567	334
		0.1	0.707	0.560	0.730	4611	1329	83057	12491	18082	758	333
Density	Initial Covariance	15	0.699	0.566	0.730	4494	1518	81942	13036	19386	569	291
		100	0.625	0.761	0.636	4363	1646	80024	13538	21169	704	366
		0.5	0.680	0.565	0.714	4432	1539	81294	12754	19993	610	265
Extraction Threshold		0.7	0.688	0.561	0.728	4452	1536	81625	12125	19691	581	287
		0.9	0.698	0.565	0.733	4495	1487	82057	11913	19192	648	295

is provided by the author of CenterPoint², and the challenge organizer provides the PointPillars³ and Megvii⁴ results. As expected, our experiments show that the tracking performances are commensurate to the quality of the detection input. The best performance is achieved with the CenterPoint detector input for each tested tracker, and the worst performance is achieved with the PointPillars detector.

2) *Computational Resource Constraints*: The marginal association probability computation of JPDA [24] is NP-hard. There is a polynomial-time approximation to such a problem [43], but it is not implemented for our tracker evaluation. The cardinality distribution computation of CPHD has $\mathcal{O}(n^3)$ complexity, where n is the cardinality of the multi-object state. For the nuScenes dataset, the maximum detection for each frame is 500. Such a large number of detection inputs would strain JPDA and CPHD computation. It is observed that the programs would be automatically terminated due to memory limitations. It is possible that the computational constraint can be circumvented by defining a smaller gating region or

with a more aggressive pruning scheme. However, such an alternative implementation would render the filter comparison unfair. Therefore, the tracking results for the JPDA and CPHD filters are not shown and denoted as N/A in TABLE I.

3) *Erroneous Modelling Assumption*: In Section III-C, the measurement model assumes that the clutter generation process is independent of the generation process of the valid detection. However, Fig. 6 demonstrates a case where this modelling assumption is violated. The tracking result is likely to be improved if proper modelling assumption are adopted.

4) *Performance of PHD Filter and TO-PMB Filter*: The set of parameters is adjusted for the PMBM filters. The performance of PHD and TO-PMB filters under this set of parameters is far from their theoretical level of performance. In theory, the performance of GNN-PMB should be between TO-PMB and PMBM. However, that is not what is observed. The PHD filter and TO-PMB implemented with LBP filter performance are likely to be improved with carefully calibrated parameters. It warrants further study in future works.

Gaussian implementations of TO-PMB suffer from the coalescence problem where multiple objects move in close proximity. This effect is demonstrated by Fig. 7.

²<https://tinyurl.com/48hskukf>

³<https://www.nuscenes.org/data/detection-pointpillars.zip>

⁴<https://www.nuscenes.org/data/detection-megvii.zip>

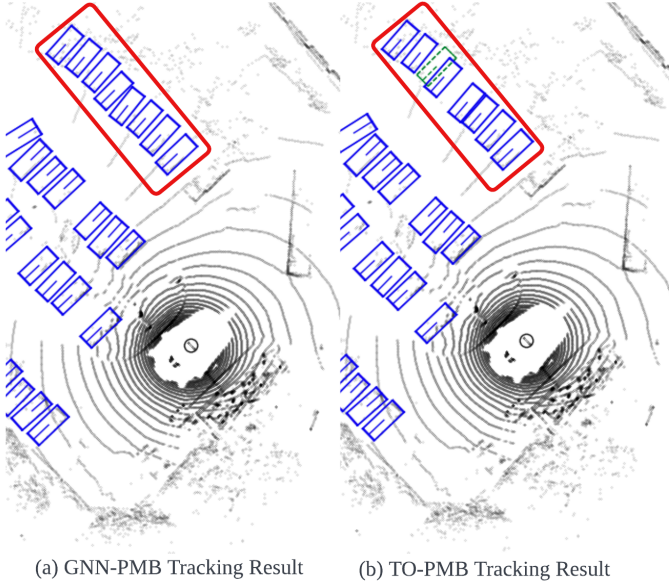


Fig. 7: The Coalescence Problem of the TO-PMB Filter. The coalescence problem refers to the phenomenon that multiple tracked objects are merged into one tracked object. It is known that the TO-PMB would suffer from the coalescence problem when multiple objects move in close proximity. This figure demonstrates the coalescence problem of the TO-PMB filter by comparing the tracking result of the same frame from both the GNN-PMB tracker and the TO-PMB tracker. In this scene, the vehicle goes through a parking lot, where the parked vehicles are tightly packed. The grey dots are the LiDAR point clouds. The blue bounding boxes are the TP object. The green bounding box with dashed line is the FN object, i.e., the object indeed exists but has not been tracked. Subfigure (a) shows the tracking result of the GNN-PMB filter. Subfigure (b) shows the tracking result of the TO-PMB filter. The part demonstrating the coalescence problem of the TO-PMB filter is enclosed with a red rectangle. In this frame, there should have 8 parked cars inside the red triangle. The GNN-PMB filter correctly tracked the 8 parked cars, but the TO-PMB filter only tracked 7 parked cars. In the result provided by the TO-PMB filter, the erroneous position of the 3rd tracked car is a weighted average of the correct positions of the 3rd and the 4th parked car. In this frame, the two objects are merged into one.

5) *Cascading Failure of PMBM Filter*: The GNN-PMB filter and the PMBM filter share the same parameters, but the former achieves an AMOTA score of 9.612% higher than that of the latter with the CenterPoint detector. The performance disparity is likely due to the fact that for the PMBM filter, faulty local hypotheses would persist for more frames, whereas the unlikely associations would not be propagated by the GNN-PMB filter, as demonstrated by Fig. 8.

D. Ablation Study of Filter Parameters

By tuning the parameters which have been introduced in Section V-C, the proposed GNN-PMB tracker achieves the highest performance. In this section, the ablation studies of parameter tuning process is explained, as shown in TABLE II.

1) *Detection Score Threshold*: The first row of TABLE II indicates that discarding the bounding box with a pre-determined detection score threshold would result in a lower AMOTA score. When the detection score threshold is set to be 0.1, 0.2, 0.3, the AMOTA score are 0.707, 0.672 and

0.625 respectively. Most noticeably, the recall decreases, and the fragmented trajectories increase as the detection score threshold increases.

The TP score of the three detection thresholds is 83088, 80971, and 80601, respectively. It means there are 2117 valid detection with detection score between 0.1 and 0.2. There are 370 valid detection with detection score between 0.2 and 0.1. The number of ground truths for the nuScenes dataset is 101897. This means there are 2.08% valid detection have detection score between 0.1 and 0.2, and there are 0.363% valid detection have detection score between 0.2 and 0.3.

Specifically, the fragmented trajectories increased by 172, from 328 to 500, when the detection score threshold increased from 0.2 to 0.3. At least 172 of the 370 valid detection with detection scores between 0.2 and 0.3 are related to the id continuity of trajectories. At least 52.4% of the valid detection with detection scores between 0.2 and 0.3 are crucial information to id continuity.

However, that is not the case when the detection score threshold increases from 0.1 to 0.2. In that case, the fragmented trajectories decreased by 13 from 341 to 328. When the detection score threshold is set to be 0.2, there are only 4391 mostly tracked trajectories, a 215 decrease from the 4606 mostly tracked trajectories when the threshold is set to be 0.1. Therefore, the decrease in fragmented trajectory is simply an artefact of the fact that there are fewer mostly tracked trajectories.

Our experiment result suggests that crucial information for trajectory continuity is contained in detection with a detection score lower than 0.3. Trajectory continuity is essential to later modules such as trajectory prediction and motion planning. Our observation shows that rather than applying the law of parsimony and pruning the detection with a low detection score, the output of the LiDAR 3D object detector should be provided to the MOT tracker in its entirety.

2) *NMS Threshold*: Setting the NMS threshold to 0.1, which discards the majority of overlapping detected bounding boxes even if only a small portion of overlap occurs, yields an AMOTA score of 0.707 with CenterPoint as the object detector. In contrast, since keeping almost all the overlapped detected bounding boxes as input of GNN-PMB tracker, by setting NMS threshold as 0.98, a lower AMOTA score 0.68 is obtained. Our observation that a basic NMS preprocess operation can achieve an AMOTA scoring difference of 0.27, denotes that only the detected bounding boxes have least overlap with each other, should be used as input to the tracker.

3) *Poisson Birth Density*: As discussed in section V-C, a proper initialization of Poisson birth density is critical prior for tracking the new birth object. On one hand, when the initial covariance of Gaussian component raises from 15 to 100, the AMOTA score is reduced from 0.699 to 0.625 and the related AMOTP score climbs from 0.566 to 0.761. Beware that the greater the AMOTP, the less accurate the output of tracker is. It is quite reasonable since as the covariance grows, the estimation uncertainty would also increase, thus leading to the rapid performance degradation.

On the other hand, the weight of Gaussian component which is part of the intensity of the Poisson process also plays a

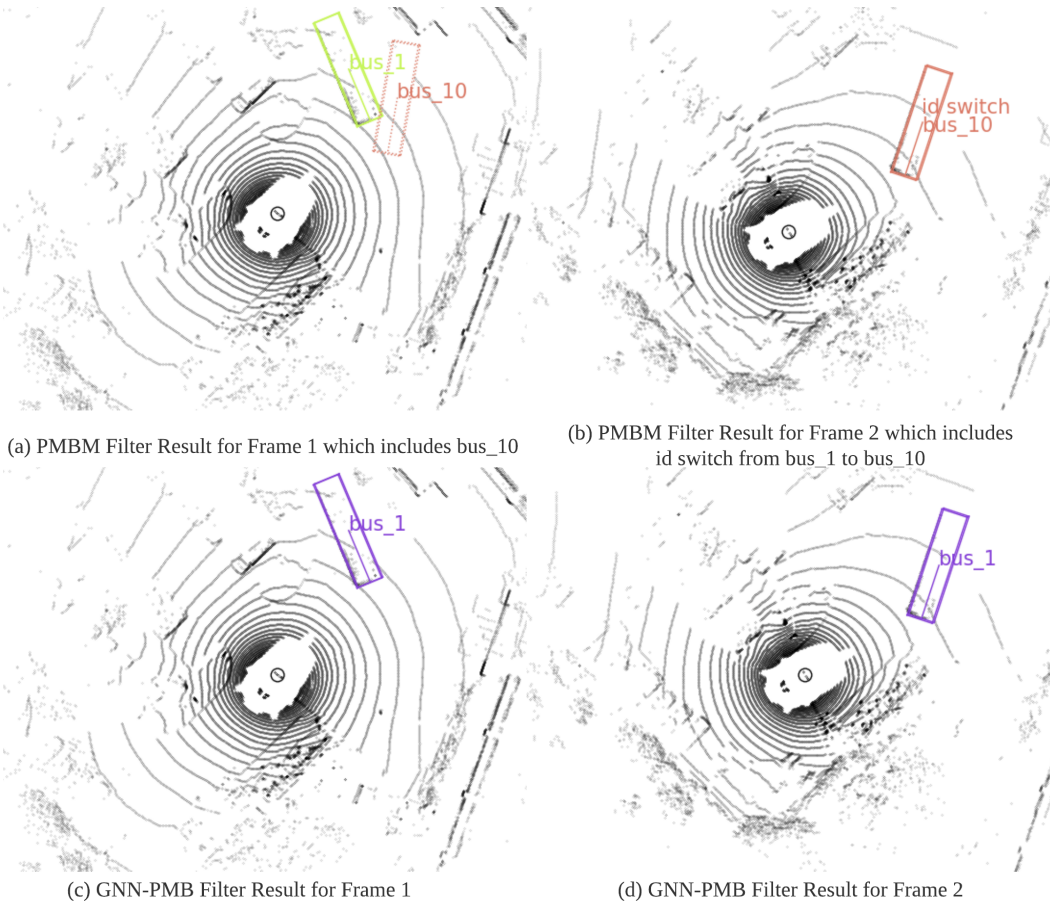


Fig. 8: Cascading Failure of the PMBM filter. This figure compares the tracking result between the PMBM filter and the GNN-PMB filter. In subfigure (a), bus_{10} represented in dash bounding box is actual a false alarm track. The track of bus_{10} is sustained by the PMBM filter, thus leading to an ID switch where the ID of the valid track changed from bus_1 to bus_{10} in the later frame, as illustrated in subfigure (b). These two errors are a series of cascading failures because the PMBM filter propagates K best global hypotheses. In the GNN-PMB filter, however, only the valid track for bus_1 is registered, and correctly maintained the same track ID for bus_1 in the following frame, as illustrated by subfigure (c) and (d).

key role for tracking the new birth objects. When the weights increases, measurement is more likely to be construed as originating from a new object than an existing object since the cost of being associated with a new object would decrease. On one extreme where the weight is too large, every measurement would be interpreted as the initial detection of a new track. On the other extreme, where the weight is too small, the measurements would always be associated with existing tracks and no new tracks would be initiated. According to the ablation study, the AMOTA decreases as the weight decreases, while the ID switch varies in the different pace as the weight varies. As a consequence, such observation demonstrates that finding a suitable value for the weight of Gaussian component to fit the statistics of object birth in the nuScenes dataset is important.

4) *Extraction Threshold*: Since the existence probability of Bernoulli component signifies how probable a object exists, precisely selecting the extraction threshold of it becomes vital for the final estimation of object states. According to our ablation investigation, raising the extraction threshold increases AMOTA, MT, and TP while lowering ML, FP, and FN. This result reveals that preserving the Bernoulli components with a high enough existence probability would result in more

accurate track estimation.

E. Performance Comparison between Our GNN-PMB Tracker using LiDAR Only and Other State-Of-The-Art Methods

1) *Performance Comparison with State-of-The-Art Model-based LiDAR Trackers using LiDAR Only*: In the nuScenes test dataset, our proposed LiDAR only tracker, GNN-PMB, is compared against various model-based LiDAR only trackers in TABLE III. Among the model-based trackers, the proposed GNN-PMB tracker receives the highest AMOTA score, which is 0.678, 4.95% percent higher than the second-best model-based tracker. Regarding AMOTP, the GNN-PMB tracker achieves a score of 0.560, which is only 0.01 worse than that of SimpleTrack, and it is the second-best AMOTP score amongst all compared model-based trackers. However, other trackers use all the 3D information provided by the object detector as input of the tracker, GNN-PMB tracker only utilises the x and y coordinate in the global frame as input. Such experiment result indicates that more input information to the MOT tracker does not automatically translate to better tracking performance. Comparable or superior tracking performance can still be achieved with less input information. Our proposed

TABLE III: Tracking Results of Our Proposed Method and Different Model-Based Trackers using LiDAR on nuScenes

Method	AMOTA↑	AMOTP↓	MT↑	ML↓	TP↑	FP↓	FN↓	IDS↓	FRAG↓
AB3DMOT (IROS 2020)* [1]	0.151	1.501	1006	4428	34808	15088	75730	9027	2557
StanfordIPRL-TRI (NeurIPS Workshop 2019)* [6]	0.550	0.798	4294	2184	85399	17533	33216	950	776
RFS-M3 (ICRA 2021)* [15]	0.619	0.752	5107	1878	90872	16728	27168	1525	856
CBMOT-LiDAR (IROS 2021)* [14]	0.649	0.592	5319	1966	94916	16469	24092	557	450
SimpleTrack (Arxiv 2021)* [7]	0.668	0.550	5476	1780	95539	17514	23451	575	591
BPTracker (Proceedings of the IEEE 2018)* [8]	0.646	0.606	5186	2259	95053	18581	24358	154	221
ImmortalTracker (Arxiv 2021)* [12]	0.677	0.599	5565	1669	96584	18012	21661	320	477
GNN-PMB (2Hz, Our)*	0.678	0.560	5698	1622	97274	17071	21521	770	431
PF-MOT tracker (ICRA 2022)** [44]	0.682	N/A	N/A	N/A	N/A	N/A	N/A	N/A	N/A
GNN-PMB (2Hz, Our)**	0.707	0.560	4608	1347	83134	12362	18113	650	345

* The metrics are reported on the nuScenes test set.

** The metrics are reported on the nuScenes validation set.

TABLE IV: Tracking Results of Our Proposed Method and Different Learning based Trackers using LiDAR on nuScenes

Method	AMOTA↑	AMOTP↓	MT↑	ML↓	TP↑	FP↓	FN↓	IDS↓	FRAG↓
SimTrack (ICCV 2021)* [16]	0.645	0.681	5063	1986	92093	17443	26430	1042	472
OGR3MOT (IEEE RAL 2022)* [17]	0.656	0.620	5278	2094	95264	17877	24013	288	371
NEBP (Arxiv 2022)* [18]	0.673	0.586	5380	2126	97023	19535	22380	162	256
GNN-PMB (2Hz, Our)*	0.678	0.560	5698	1622	97274	17071	21521	770	431
TransMOT (IEEE IV 2022)** [45]	0.674	0.754	2096	N/A	N/A	9449	14071	1403	N/A
GNN-PMB (2Hz, Our)**	0.849	0.387	2762	668	49182	6140	8791	344	170

* The metrics are reported on the nuScenes test set.

** The metrics are reported on the nuScenes validation set for car.

TABLE V: Tracking Results of Our Proposed Method and Different Trackers using LiDAR and Camera Fusion on nuScenes Test Set

Method	AMOTA↑	AMOTP↓	MT↑	ML↓	TP↑	FP↓	FN↓	IDS↓	FRAG↓
Probabilistic3DMM (ICRA 2021)* [9]	0.655	0.617	5494	1557	95199	18061	23323	1043	717
EagerMOT (ICRA 2021)* [10]	0.677	0.550	5303	1842	93484	17705	24925	1156	601
CBMOT (IROS 2021)* [14]	0.676	0.518	5420	1654	96028	21604	22828	709	1015
AlphaTrack (IROS 2021)* [19]	0.693	0.585	5560	1744	95851	18421	22996	718	480
GNN-PMB (2Hz, Our)**	0.678	0.560	5698	1622	97274	17071	21521	770	431

* All trackers are based fusion of LiDAR and camera.

** Our tracker is based on LiDAR only.

method also outperforms all the model-based trackers in MT, ML, TP, and FN, with the FP score coming in second only to CBMOT. Notably, the GNN-PMB tracker achieves an MT score of 5698. Even with lower frequency input (i.e. 2Hz), the GNN-PMB tracker still successfully tracked 4.05% more tracks than does SimpleTrack, which employed detection at 10Hz as the input. Moreover, the GNN-PMB tracker is even superior on ImmortalTracker, which is an offline smoother refines the trajectory with more accumulated information in the future, though it is impractical in the real-world system for online tracking. Another recent proposed LiDAR-only model-based tracker, PF-MOT tracker, only reported performances partially in the nuScenes validation dataset rather than the test dataset, thus we can only compare with it on the validation dataset. The result shows that GNN-PMB tracker achieves an AMOTA of 0.707, which is also higher than the 0.682 AMOTA achieved by the PF-MOT tracker.

The drawback of GNN-PMB tracker are the higher IDS and FRAG compared to BPTracker, which has only 154 ID switches and 221 fragments. However, considering fairly low values in MT, the low ID switches achieved by the BPTracker could be an artefact from having less mostly tracked tracks.

2) *Performance Comparison with Data-Driven State-Of-The-Art Trackers using LiDAR Only:* We also compare our proposed GNN-PMB with learning-based state-of-the-art trackers. As shown by TABLE IV, our proposed GNN-PMB tracker achieves the best performance in all evaluation metrics other than IDS and FRAG when it is compared with the data-driven trackers. The NEBP tracker and the OGR3MOT Tracker have low ID switches for the same reason as the BPTracker has a low IDS score, as explained in Section VI-E1.

In particular, our proposed GNN-PMB tracker achieves an AMOTP score of 0.56, which is 0.026 better than that of the NEBP tracker, the second best tracker among all the learning based trackers. The AMOTP score indicates that the GNN-PMB tracker can provide more accurate position information than the NEBP tracker.

3) *Performance Comparison with State-Of-The-Art Trackers using LiDAR and Camera Fusion:* To demonstrate the advantages of our proposed GNN-PMB tracker even further, comparison with state-of-the-art trackers using LiDAR and camera fusion is also shown. In contrast to state-of-the-art trackers utilising LiDAR and camera fusion, our proposed GNN-PMB tracker only uses LiDAR to obtain comparable tracking performance on AMOTA and AMOTP, and is even

superior on MT, TP, FP, and FN, as shown in TABLE V. Such result shows enormous potential to increase performance even further when GNN-PMB tracking framework is extended into settings with fusion of LiDAR and camera.

VII. CONCLUSION AND FUTURE WORK

In this paper, a systematical comparison between different random vector Bayesian filters and RFS filters are held on the nuScenes validation dataset. Based on this, a simple but effective online multi-object tracker in a uniform framework, GNN-PMB, which only requires the x and y coordinates of the bounding box in the global frame are used as input, is proposed. Such a simple MOT scheme achieved the state-of-the-art performance on the nuScenes benchmark dataset. The performance of our proposed method can be potentially further improved with simply modification, such as the providing 3D state information as input, employing both LiDAR and camera as sensor modalities, and meta-learning-based parameter auto-tuning module. For the future work, downstream tasks such as trajectory prediction and motion planning should also be incorporated into the assessment of the multi-object trackers, to design a more robust multi-object tracker in end-to-end manner.

REFERENCES

- [1] X. Weng, J. Wang, D. Held, and K. Kitani, "3d multi-object tracking: A baseline and new evaluation metrics," in *2020 IEEE/RSJ International Conference on Intelligent Robots and Systems (IROS)*. IEEE, 2020, pp. 10 359–10 366.
- [2] S. J. Davey, M. G. Rutten, and B. Cheung, "A comparison of detection performance for several track-before-detect algorithms," *EURASIP Journal on Advances in Signal Processing*, vol. 2008, pp. 1–10, 2007.
- [3] Z. Lu, V. Rathod, R. Votel, and J. Huang, "Retinatrack: Online single stage joint detection and tracking," in *Proceedings of the IEEE/CVF conference on computer vision and pattern recognition*, 2020, pp. 14 668–14 678.
- [4] Y. Zhang, C. Wang, X. Wang, W. Zeng, and W. Liu, "Fairmot: On the fairness of detection and re-identification in multiple object tracking," *International Journal of Computer Vision*, pp. 1–19, 2021.
- [5] Y. Zhang, P. Sun, Y. Jiang, D. Yu, Z. Yuan, P. Luo, W. Liu, and X. Wang, "Bytetrack: Multi-object tracking by associating every detection box," *arXiv preprint arXiv:2110.06864*, 2021.
- [6] H. Kuang Chiu, A. Prioletti, J. Li, and J. Bohg, "Probabilistic 3d multi-object tracking for autonomous driving," *ArXiv, vol. abs/2001.05673*, 2020.
- [7] Z. Pang, Z. Li, and N. Wang, "Simpletrack: Understanding and rethinking 3d multi-object tracking," *arXiv preprint arXiv:2111.09621*, 2021.
- [8] F. Meyer, T. Kropfreiter, J. L. Williams, R. Lau, F. Hlawatsch, P. Braca, and M. Z. Win, "Message passing algorithms for scalable multitarget tracking," *Proceedings of the IEEE*, vol. 106, no. 2, pp. 221–259, 2018.
- [9] H.-k. Chiu, J. Li, R. Ambruş, and J. Bohg, "Probabilistic 3d multi-modal, multi-object tracking for autonomous driving," in *2021 IEEE International Conference on Robotics and Automation (ICRA)*. IEEE, 2021, pp. 14 227–14 233.
- [10] A. Kim, A. Osep, and L. Leal-Taixé, "Eagermot: 3d multi-object tracking via sensor fusion," in *2021 IEEE International Conference on Robotics and Automation (ICRA)*. IEEE, 2021, pp. 11 315–11 321.
- [11] Z. Zheng, P. Wang, W. Liu, J. Li, R. Ye, and D. Ren, "Distance-iou loss: Faster and better learning for bounding box regression," in *Proceedings of the AAAI conference on artificial intelligence*, vol. 34, no. 07, 2020, pp. 12 993–13 000.
- [12] Q. Wang, Y. Chen, Z. Pang, N. Wang, and Z. Zhang, "Immortal tracker: Tracklet never dies," *arXiv preprint arXiv:2111.13672*, 2021.
- [13] H. Wu, W. Han, C. Wen, X. Li, and C. Wang, "3d multi-object tracking in point clouds based on prediction confidence-guided data association," *IEEE Transactions on Intelligent Transportation Systems*, vol. 23, pp. 5668–5677, 2022.
- [14] N. Benbarka, J. Schröder, and A. Zell, "Score refinement for confidence-based 3d multi-object tracking," *2021 IEEE/RSJ International Conference on Intelligent Robots and Systems (IROS)*, 2021.
- [15] S. Pang, D. Morris, and H. Radha, "3d multi-object tracking using Random Finite Set-based multiple measurement models filtering (RFS-M 3) for autonomous vehicles," in *2021 IEEE International Conference on Robotics and Automation (ICRA)*. IEEE, 2021, pp. 13 701–13 707.
- [16] C. Luo, X. Yang, and A. Yuille, "Exploring simple 3d multi-object tracking for autonomous driving," *International Conference on Computer Vision (ICCV)*, 2021.
- [17] J.-N. Zaeck, D. Dai, A. Liniger, M. Danelljan, and L. V. Gool, "Learnable online graph representations for 3d multi-object tracking," *IEEE Robotics and Automation Letters*, vol. 7, pp. 5103–5110, 2022.
- [18] M. Liang and F. Meyer, "Neural enhanced belief propagation for data association in multiobject tracking," *arXiv preprint arXiv:2203.09948*, 2022.
- [19] Y. Zeng, C. Ma, M. Zhu, Z. Fan, and X. Yang, "Cross-modal 3d object detection and tracking for auto-driving," in *2021 IEEE/RSJ International Conference on Intelligent Robots and Systems (IROS)*. IEEE, 2021, pp. 3850–3857.
- [20] R. P. Mahler, *Statistical multisource-multitarget information fusion*. Artech House Norwood, MA, USA, 2007, vol. 685.
- [21] S. S. Blackman and R. Popoli, *Design and analysis of modern tracking systems*. Artech House Publishers, 1999.
- [22] T. Fortmann, Y. Bar-Shalom, and M. Scheffe, "Sonar tracking of multiple targets using joint probabilistic data association," *IEEE journal of Oceanic Engineering*, vol. 8, no. 3, pp. 173–184, 1983.
- [23] Y. Bar-Shalom, F. Daum, and J. Huang, "The probabilistic data association filter," *IEEE Control Systems Magazine*, vol. 29, no. 6, pp. 82–100, 2009.
- [24] D. Reid, "An algorithm for tracking multiple targets," *IEEE transactions on Automatic Control*, vol. 24, no. 6, pp. 843–854, 1979.
- [25] B.-N. Vo and W.-K. Ma, "The Gaussian Mixture Probability Hypothesis Density Filter," *IEEE Transactions on Signal Processing*, vol. 54, pp. 4091–4104, 2006.
- [26] B.-T. Vo, B.-N. Vo, and A. Cantoni, "The Cardinalized Probability Hypothesis Density Filter for Linear Gaussian Multi-Target Models," *2006 40th Annual Conference on Information Sciences and Systems*, pp. 681–686, 2006.
- [27] Á. F. García-Fernández, J. L. Williams, K. Granström, and L. Svensson, "Poisson Multi-Bernoulli Mixture Filter: Direct derivation and implementation," *IEEE Transactions on Aerospace and Electronic Systems*, vol. 54, pp. 1883–1901, 2018.
- [28] J. L. Williams, "Marginal multi-Bernoulli filters: RFS derivation of MHT, JIPDA, and association-based MeMBer," *IEEE Transactions on Aerospace and Electronic Systems*, vol. 51, no. 3, pp. 1664–1687, 2015.
- [29] K. Panta, D. E. Clark, and B.-N. Vo, "Data association and track management for the Gaussian mixture probability hypothesis density filter," *IEEE transactions on aerospace and electronic systems*, vol. 45, no. 3, pp. 1003–1016, 2009.
- [30] Á. F. García-Fernández and L. Svensson, "Trajectory PHD and CPHD filters," *IEEE Transactions on Signal Processing*, vol. 67, no. 22, pp. 5702–5714, 2019.

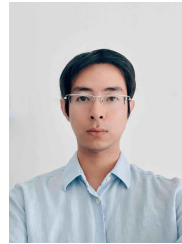
- [31] K. Granström, L. Svensson, Y. Xia, J. Williams, and Á. F. García-Fernández, “Poisson multi-Bernoulli mixture trackers: Continuity through random finite sets of trajectories,” in *2018 21st International Conference on Information Fusion (FUSION)*. IEEE, 2018, pp. 1–5.
- [32] S. S. Blackman, “Multiple Hypothesis Tracking for multiple target tracking,” *IEEE Aerospace and Electronic Systems Magazine*, vol. 19, pp. 5–18, 2004.
- [33] S. Oh, S. Russell, and S. Sastry, “Markov chain Monte Carlo data association for multi-target tracking,” *IEEE Transactions on Automatic Control*, vol. 54, no. 3, pp. 481–497, 2009.
- [34] D. F. Crouse, “On implementing 2D rectangular assignment algorithms,” *IEEE Transactions on Aerospace and Electronic Systems*, vol. 52, no. 4, pp. 1679–1696, 2016.
- [35] J. L. Williams and R. A. Lau, “Approximate evaluation of marginal association probabilities with belief propagation,” *IEEE Transactions on Aerospace and Electronic Systems*, vol. 50, pp. 2942–2959, 2014.
- [36] Y. Xia, K. Granstrom, L. Svensson, and Á. F. García-Fernández, “Performance evaluation of multi-Bernoulli conjugate priors for multi-target filtering,” in *2017 20th International Conference on Information Fusion (Fusion)*. IEEE, 2017, pp. 1–8.
- [37] J. Smith, F. Particke, M. Hiller, and J. Thielecke, “Systematic analysis of the PMBM, PHD, JPDA and GNN multi-target tracking filters,” in *2019 22th International Conference on Information Fusion (FUSION)*. IEEE, 2019, pp. 1–8.
- [38] A. Geiger, P. Lenz, C. Stiller, and R. Urtasun, “Vision meets robotics: The kitti dataset,” *The International Journal of Robotics Research*, vol. 32, no. 11, pp. 1231–1237, 2013.
- [39] P. Sun, H. Kretschmar, X. Dotiwalla, A. Chouard, V. Patnaik, P. Tsui, J. Guo, Y. Zhou, Y. Chai, B. Caine, *et al.*, “Scalability in perception for autonomous driving: Waymo open dataset,” in *Proceedings of the IEEE/CVF conference on computer vision and pattern recognition*, 2020, pp. 2446–2454.
- [40] H. Caesar, V. Bankiti, A. H. Lang, S. Vora, V. E. Liong, Q. Xu, A. Krishnan, Y. Pan, G. Baldan, and O. Beijbom, “nuScenes: A multimodal dataset for autonomous driving,” in *Proceedings of the IEEE/CVF conference on computer vision and pattern recognition*, 2020, pp. 11 621–11 631.
- [41] M.-F. Chang, J. Lambert, P. Sangkloy, J. Singh, S. Bak, A. Hartnett, D. Wang, P. Carr, S. Lucey, D. Ramanan, *et al.*, “Argoverse: 3d tracking and forecasting with rich maps,” in *Proceedings of the IEEE/CVF Conference on Computer Vision and Pattern Recognition*, 2019, pp. 8748–8757.
- [42] K. Bernardin, A. Elbs, and R. Stiefelhofen, “Multiple object tracking performance metrics and evaluation in a smart room environment,” in *Sixth IEEE International Workshop on Visual Surveillance, in conjunction with ECCV*, vol. 90, no. 91. Cite-seer, 2006.
- [43] S. Oh and S. Sastry, “A polynomial-time approximation algorithm for joint probabilistic data association,” in *Proceedings of the 2005, American Control Conference, 2005*. IEEE, 2005, pp. 1283–1288.
- [44] N. F. Wen Tao, Yanyong Zhang, “PF-MOT: Probability fusion based 3d multi-object tracking for autonomous vehicles,” *IEEE International Conference on Robotics and Automation (ICRA)*, 2022.
- [45] F. Ruppel, F. Faion, C. Gläser, and K. Dietmayer, “Transformers for multi-object tracking on point clouds,” *IEEE Intelligent Vehicles Symposium (IV)*, 2022.



Jianan Liu received his B.Eng. degree in Electronics and Information Engineering from Huazhong University of Science and Technology, Wuhan, China, in 2007. He received his M.Eng. degree in Telecommunication Engineering from the University of Melbourne, Australia, and his M.Sc. degree in Communication Systems from Lund University, Sweden, in 2009 and 2012, respectively. Jianan has over ten years of experience in software and algorithm design and development. He has held senior R&D roles in the AI consulting, automotive, and telecommunication industries. His research interests include applying statistical signal processing and deep learning for medical image processing, wireless communications, IoT networks, indoor sensing, and outdoor perception using a variety of sensor modalities like radar, camera, LiDAR, WiFi, etc.



Liping Bai received her M.Eng. degree in Instrument Engineering from Nanjing University of Posts and Telecommunications, Nanjing, China, in 2021. She is currently pursuing her Ph.D. in Automation and Control Engineering at Beihang University, Beijing, China. Her research interest is the intersection between control theory and machine learning.



Yuxuan Xia was born in Wuhan, China, in 1993. He received the B.Sc. degree in engineering of Internet of Things from Jiangnan University, Wuxi, China, in 2015 and the M.Sc. degree in communication engineering in 2017 from the Chalmers University of Technology, Gothenburg, Sweden, where he is currently working toward the Ph.D. degree with the Department of Electrical and Engineering. His main research interests include multi-object tracking and sensor fusion, especially for extended objects. He has co-organised tutorials on multi-object tracking at the Information Fusion conference.



Tao Huang (SM'20) received his Ph.D. degree in Electrical Engineering from The University of New South Wales, Sydney, Australia. Currently, Dr. Huang is a lecturer in Electronic Systems and IoT Engineering at James Cook University, Cairns, Australia. He was an Endeavour Australia Cheung Kong Research Fellow, a visiting scholar at The Chinese University of Hong Kong, a research associate at the University of New South Wales, and a postdoctoral research fellow at James Cook University. He has co-authored a Best Paper Award from the 2011 IEEE WCNC, Cancun, Mexico. He is currently serving as the MTT-S/Com Vice-Chair and Young Professionals Representative for the IEEE Northern Australia Section. His research interests include deep learning, smart sensing, computer vision, pattern recognition, wireless communications, and IoT security.



Bing Zhu (Member, IEEE) was born in Wuhan, P.R. China. He received his BS and Ph.D. degrees in Control Theory and Applications from Beihang University, Beijing, P.R. China, in 2007 and 2013, respectively. He was with the University of Pretoria, Pretoria, South Africa, as a postdoctoral fellow supported by Vice-Chancellor Postdoctoral Fellowship from 2013 to 2015. He was with Nanyang Technological University, Singapore, as a research fellow from 2015 to 2016. He joined Beihang University, Beijing, P.R. China as an associate professor in 2016. Dr. Zhu serves as an Associate Editor for Acta Automatica Sinica. His research interests include model predictive control, smart sensing for UAV and UGV, and demand-side management for new energy systems.